A Theoretical Model for RF Ablation of Kidney Tissue and Its Experimental Validation

Mihaela Pop[1], Sean R.H. Davidson[2], Mark Gertner[2,3], Michael A.S. Jewett[4], Michael D. Sherar[1,2], and Michael C Kolios[1,3]

[1] Department of Medical Biophysics, University of Toronto, Toronto, Canada
mihaela.pop@utoronto.ca
[2] Division of Biophysics and Bioimaging, University Health Network, Toronto, Canada
[3] Department of Physics, Ryerson University, Toronto, Canada
[4] Division of Surgical Oncology, University Health Network, Toronto, Canada

Abstract. Radio-frequency (RF) ablation is a minimal invasive thermal therapy, currently considered as an alternative to surgery to eradicate small solid kidney tumors. Our aim is to understand the kinetics of thermal lesion growth in kidney tissue exposed to RF energy by taking into account dynamic time-temperature changes in electrical properties of multiple tissues (i.e. kidney, surrounding fat, muscle). We present a computer model designed to calculate the voltage distribution and the temperature rise in kidney. The model further calculates the RF lesion size based on kinetic processes, which correctly describe coagulative necrosis process. The simulated transient temperatures and lesion size were experimentally validated with good agreement in a porcine kidney model, *ex vivo*. The expected increase in electrical conductivity of kidney (approximately 3 times) during heating resulted in predicted lesion width and depth that were larger (by as much as 20% and 30% respectively) than those predicted for constant properties. Simulation results also show how the lesion size and shape can be affected by the proximity to the RF electrode of a surrounding layer of fat, which acts as an electro-thermal insulator. The results of this pre-clinical investigation may be useful for treatment planning of RF thermal therapy of kidney tumours.

Keywords: computer modelling, radio-frequency ablation, kidney, thermal damage.

1 Introduction

Radio-frequency ablation (RF ablation) is currently being investigated clinically as a minimally invasive alternative to surgery for the treatment of solid renal masses of about 3cm in diameter, but the success rate is controversial. Clinical studies showed that the size and shape of RFA renal lesions are not reproducible [1]. The aim of the RFA is to elevate tissue temperature beyond 50°C, where protein coagulation causes cell death [2]. Computer models could help to better understand the kinetics of lesion formation and to predict the extent of necrosis (i.e., lesion).

F. Bello and S. Cotin (Eds.): ISBMS 2010, LNCS 5958, pp. 119–129, 2010.

Theoretical models incorporate electrical and thermal factors influencing the lesion growth could. Any change in tissue electrical conductivity, σ, is expected to affect the RF energy deposition which is known to be directly proportional to electrical conductivity of tissue, and, consequently, the temperature distribution and tissue damage [3]. We have previously demonstrated that σ changes significantly for kidney and fat tissues at ablation frequencies (i.e. 460 kHz) during heating to high temperatures [4]. These changes were due to reversible, temperature–dependent and permanent structural changes (e.g. protein coagulation, melting of fatty acids) that occur during heating. Such dynamic changes characterize the thermal transitions and are very important for biological tissues. Computer models have been developed to predict the RF energy deposition in tissue and subsequent temperature rise in heart and liver tissue for different RF electrode designs, as summarized in [5]. Some models have included reversible, temperature-dependent changes in electrical conductivity of liver, with coefficients derived from NaCl solutions [6]. Permanent, irreversible changes of electrical properties during heating could play an important role in the theoretical predictions, and thus, they should be taken into account. Only one study [7] has incorporated such dynamic changes into a model of RF kidney ablation, but the validation of the predictions was limited to a few point temperature probes. Moreover, these authors compared the simulated lesion size with the experimental lesion based on the 42ºC iso-dose temperature, although it is well known that the critical temperature where protein coagulation starts to cause the death of cells is beyond 50°C. For kidney tissue, we previously demonstrated [4], via gross examination and histological analysis, that low temperatures (i.e. 42-47ºC) cannot be associated with irreversible thermal effects.

In this paper, we present a computer model that includes the temperature-dependant as well as permanent changes in kidney tissue electrical conductivity due to thermal damage. We predicted this damage using the Arrhenius formalism which appropriately describes the coagulative necrosis. In addition, layers of fat and fat were incorporated into the computational domain, to mimic the anatomy of kidney. Our calculations were validated by measuring the temperature rise during RF heating in pig kidney, *ex vivo*, using a thermographic technique, which is superior to point temperature sensors as it offers surface iso-temperature maps instead of sparse point measurements. The calculated extent of damage was validated by comparison with the size of RF lesions also created in porcine kidney tissue.

2 Methodology

2.1 Mathematical Model and Computer Implementation

Our numerical model contains three components: 1) calculation of the RF energy absorbed by the tissue using electromagnetic field theory; 2) calculation of the transient tissue temperatures using Pennes bio-heat equation; and 3) calculation of the extent of the thermal damage using the Arrhenius formalism. For the first step (i.e., modelling of the RF energy distribution), the RF energy deposited in tissue can be expressed in terms of *absorbed power density* P(Wm^{-3}) and is given by [3]:

$$P = \sigma \mid E \mid^2 = \frac{\mid j \mid^2}{\sigma}, \tag{1}$$

where σ is the tissue electrical conductivity (S m^{-1}), and $\mid E \mid$ and $\mid j \mid$ are the magnitudes of the electrical field (V m^{-1}) and current density (A m^{-2}), respectively.

The electrical field $\vec{E} = -\nabla V$ can be calculated if the voltage distribution, V, is known. At the operating frequency of the RF applicator used in this study (i.e. 460 kHz), the tissue is considered source-free and the displacement currents are neglected. This is known as *quasi-static approximation*.

The voltage is calculated by solving the Laplace equation: $\nabla \cdot \sigma \nabla V = 0$ [3], for which Dirichlet boundary conditions are applied: a specified value 35.5 V rms on the electrode surface, and zero on the outer domain boundary corresponding to the ground electrode. For complex geometries there is no analytical solution for Laplace equation, therefore, we employed the finite element method (FEM).

The RF energy absorbed by the tissue in the vicinity of the electrode causes a localized rise in temperature. This thermal gradient causes thermal conduction from the electrode into the surrounding tissue. The balance of thermal energy in time and space can be modeled by the *bio-heat transfer equation* (BHTE) given in [8]:

$$\rho_t c_t \frac{\partial T}{\partial t} = P + \nabla \cdot (k_t \nabla T) - c_b w_b (T - T_b) - Q_m, \tag{2}$$

where ρ_t is the tissue mass density (g cm^{-3}), k_t is the thermal conductivity of tissue (W $cm^{-1}K^{-1}$), c_t and c_b are the specific heat of tissue and blood (J g^{-1} K^{-1}), T and T_b are the local tissue and blood temperatures (°C), w_b is the volumetric perfusion rate (g $cm^{-3}s^{-1}$), P is the heat deposited (W cm^{-3}) and Q_m is the metabolic heat (W cm^{-3}), which is very small (thus is usually neglected). To solve the BHTE, a constant temperature at the boundary of the domain was assumed. The volumetric perfusion term was set to zero in this study. Most of the physical properties were taken from [10].

Next, the degree of tissue damage at a tissue location *r*, is calculated using [9]:

$$\Omega(r,t) = \ln\left\{\frac{[C(r,0)]}{[C(r,t)]}\right\} = \int_0^t A e^{-\frac{E_a}{RT(r,\tau)}} d\tau, \tag{3}$$

where $\Omega(r,\tau)$ is the thermal damage index (dimensionless), τ denotes the exposure time (s), A is the frequency constant (s^{-1}), E_a is the activation energy (J mol^{-1}) and R is the universal gas constant (8.314 J $mol^{-1}K^{-1}$). The thermal damage is defined as the logarithm of the ratio of the original concentration of native tissue at time zero, C(r,0), to the remaining native state tissue at time τ, $C(r,\tau)$, A value of 1 for Ω represents 63% of the cells in a damaged state (e.g. cell death, protein coagulation).

A FEM solution of the coupled electro-thermal problem was implemented in a computer program that incorporated the Diffpack C++ FEM class library (inuTech GmbH, Nurnberg, Germany). The Laplace equation and BHTE were solved separately. At each time step, the power input to the tissue was calculated by the electrical solver and transferred to the thermal solver (Fig. 1).

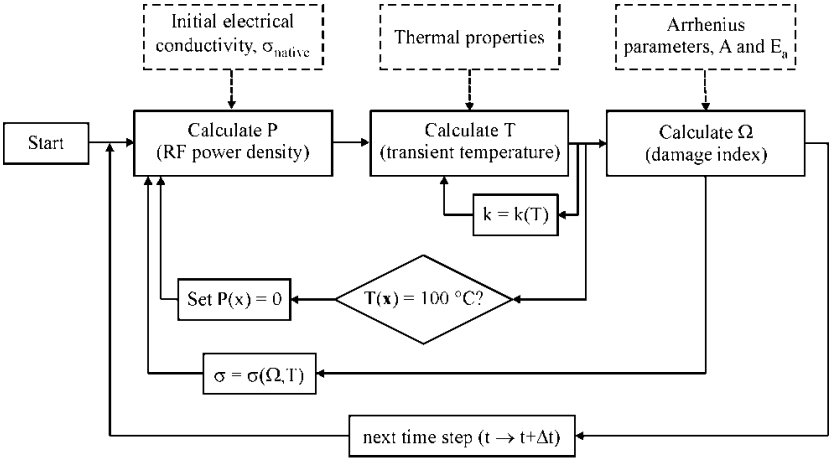

Fig. 1. Flowchart for the non-linear electro-thermal solver

The damage calculated from the thermal solver was then used to update the electrical properties in the electrical solver. The solution of the electro-thermal problem is non-linear due to the dynamic changes in tissue properties σ and k during heating. At time (t), the heat source P(x,t) is calculated and fed into the calculation for T(x,t), which is then used to determine the thermal damage Ω(x,t). Both T and Ω affect the tissue property values, which are re-evaluated *after* each time step. Then, the model re-calculates at the next time iteration (t+Δt) the heat source P(x,t+Δt) based on the new distribution for σ, then re-estimates the local temperature T(x,t+Δt) based on the new values for P and k, and calculates the accumulated thermal damage Ω(x,t+Δt). The calculation of σ is based on tissue measurements up to 78ºC [4], however σ is also known to decrease dramatically as tissue desiccates and approaches vaporization temperatures. To implement this effect, the power P was set to zero when T reached 100°C.

The temperature-dependent thermal conductivity of the tissue, *k(T)*, was calculated after each time step according to: $k(T) = k_0 \cdot [1+\beta \cdot (T(t)-T_0)]$, where k_0 is the thermal conductivity of at $T_0 = 22$ºC and β is the temperature coefficient (ºC^{-1}) [10].

A mesh of triangular elements was generated over the computational domain using Geompack (ZCS Inc., Calgary, Canada). The mesh automatically produces smaller elements around complicated structures (e.g. tissue/electrode interface, electrode tip). The treatment duration was divided into multiple time steps. After convergence tests, a time step of 0.1s and a mesh of 35048 triangular elements were used in all simulations.

Materials and tissue properties (electrical, thermal and mechanical) were included to Table 1.

Table 1. Electrical and thermal properties used in simulations: electrical conductivity σ (at 460 kHz), heat capacity *c*, thermal conductivity *k*, mass density ρ, and temperature coefficients, α and β, for electrical and thermal conductivity, respectively.

Material/Tissue [reference]	σ S cm^{-1}	c Jg^{-1} K^{-1}	k Wcm^{-1}K^{-1}	ρ_t g cm^{-3}	α %°C^{-1}	β %°C^{-1}
Electrode (stainless steel) [6]	$8x10^{4}$	$4.7x10^{-2}$	$2x10^{-1}$	8	0	0
Catheter (polyurethane) [6]	$1x10^{-7}$	1.05	$2x10^{-4}$	$7x10^{-2}$	0	0
Kidney (pig) [4] and [10]	$2.2x10^{-1}$	3.89	$4.8x10^{-3}$	1.05	1.6	0.3
Fat, porcine [4] and [10]	$2x10^{-2}$	2.6	$1.7x10^{-3}$	0.96	1.7	0.2
Muscle [10]	$3x10^{-1}$	3.9	$4.9x10^{-3}$	1.06	2.1	0.2
0.2% NaCl sol. [10]	$2.2x10^{-1}$	4.18	$5.1x10^{-3}$	1.0	2	0.2

2.2 Experimental Validation

Freshly excised porcine kidneys were used for the experimental part. The RF lesions were created using a LeVeen™ electrode (2 cm diameter tip-to tip) with eight stainless steel tines (4 mm thickness) deployed in an 'umbrella' fashion in the kidney (Fig. 2). The electrode has an insulated catheter (polyurethane, 2 mm diameter) and the needle tip has an un-insulated section (1 mm length, 2 mm diameter). The LeVeen electrode was connected to an RF 2000™ generator. The tissue electrical impedance rises when tissue desiccates the power falls to zero.

Fig. 2. RF ablation electrode (LeVeen needle, 2cm diameter; Boston Scientific, USA)

2D temperature patterns were measured using a thermographic technique. The kidneys were cut into two pieces in coronal plane and a 2cm RF electrode was placed between them; only two opposite tines were used to compare with the 2D calculation. After applying a voltage of 35.5V rms for 7s or 60 s, the top portion of the kidney was removed and the surface of the bottom part was exposed. An infrared (IR) camera (FLIR systems, model SC2000, accuracy 0.2°C) was used to measure the temperature on the exposed surface. The camera recorded continuously at a rate of 5 frames/s rate. A cooling delay between end of heating and temperature acquisition starting time was estimated to 0.5s (and was also taken into consideration in theoretical calculations).

Before each measurement, calibration measurements were made using objects of known dimensions. The 2D temperature maps were converted into contour plots using Matlab (Mathworks, CA).

For the thermal damage assessment, RF lesions were created ex vivo in porcine kidney, with and without a surrounding layer of fat. The lesions were produced by applying a power of 40W (35.5 V r.m.s.) to a 2cm electrode LeVeen electrode deployed into the kidney. The kidney was immersed in 0.2% saline solution at 37ºC (having the same electrical conductivity as kidney, 0.0022Sm^{-1}) and placed on a layer of muscle tissue that, in turn, was placed on a grounded electrode. Several lesions were also produced in kidney surrounded by a layer of fat (4-5 mm thickness) sewn to the kidney using surgical thread to ensure good contact. The lesion extent was assessed by gross pathology. The thermal lesion usually appear as a whitened area of coagulated tissue surrounded by a red rim (due to collapsed and ruptured red blood cells), beyond which tissue is normal [2]. The size of the RF ablation lesion was compared to the thermal damage predicted by simulations.

3 Results

The 2D computational domain used in simulations is shown in Fig. The 7x7 cm domain was segmented into regions (kidney, fat, muscle, etc) to replicate the experiment. The voltage solution is shown in Figsures 3b (no fat) and 3c (with fat included). An asymmetry in voltage distribution is created around the electrode tine placed in the vicinity of fat (fig 3c) because σ of fat is ~1/10 that of kidney.

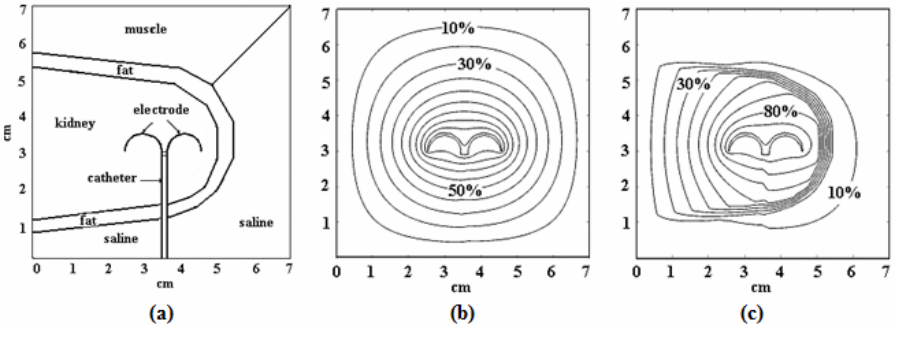

Fig. 3. The computational domain used in simulations (a). The voltage solution: (b) with the layer of fat not included, and (c) with fat surrounding the kidney.

Figure 4 shows contours of temperature measured on the exposed surface of the kidney immediately after 7s heating (4a) and 60s heating (4c). The predictions for the same heating durations are shown in Figs 4b and 4d, respectively. Both measured and predicted maximum absolute temperatures are given in Table 2.

Table 2. Maximum absolute temperature predicted and measured using the thermographic technique. Experimental results are given as mean ± standard deviation (3 or 4 experiments).

Thermal treatment time (s)	Maximum absolute temperature (°C)	
	Simulations (dynamic case)	Experiments
7s heating +		
a) 0s cooling	45.9	N/A
b) 0.5s cooling	41.1	43.6 ± 4.1 (3)
60 s heating +		
a) 0 s cooling	91.8	N/A
b) 0.5 s cooling	87.7	84.9 ± 4.0 (4)

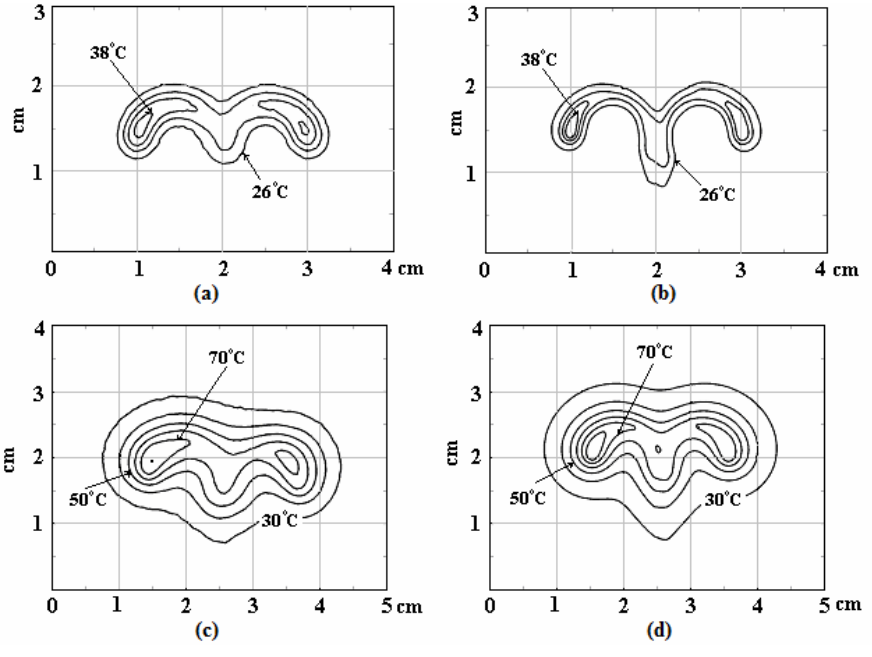

Fig. 4. Iso-temperature contours (a) measured after 7s heating, (b) predicted for 7s heating + 0.5s cooling using the dynamic properties model, (c) measured after 60s heating and (d) predicted for 60s heating + 0.5s cooling using the dynamic properties model

The measured and calculated maximum temperatures were in a good agreement for the 7s heating. However, the experimental contours (fig 4a) are slightly wider than the theoretical contours (fig. 4b). This difference may be due to the limited spatial resolution (1 mm) of the camera or to the noise in the thermographic images. The depths and widths of temperature iso-contours at 60 s (figs 4c and 4d) were in very good agreement. After 0.5 s cooling, the calculated maximum absolute temperature was 2.8°C higher than the experimental value, representing a difference of 4.5%. In all cases, the maximum temperature occurs at the electrode tip.

A comparison of the transient temperatures after 120 s of heating (plots not shown) for the 3 models, showed that for the dynamic case, an increase in σ with respect to time and temperature caused an increase in maximum P value from 2751 Wcm^{-3} to 7980 Wcm^{-3}, being maximum at the electrode tip. The dynamic model showed an increase of ~8% in both depth and width of the 50°C contour in comparison with the static model. Moreover, when the fat was included, the area encompassed by the temperature contours changed (e.g. the 50°C contour was 10% larger in width than in dynamic case) due to the thermal insulation property of the fat.

The calculated extent of damage after a 6 min thermal treatment (2 min heating + 1 min cooling + 1 min heating + 2 min cooling) is shown in Fig 5.

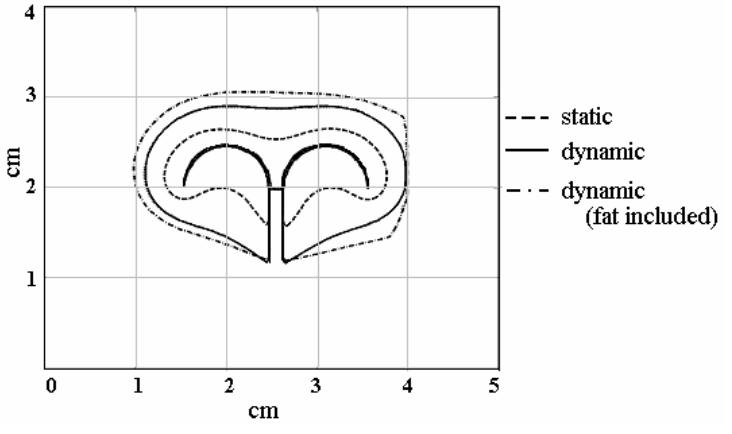

Fig. 5. RFA lesion predicted for different models; the outer line corresponds to a dynamic case with fat, the middle line to a dynamic case with no fat, and the inner line to a static case.

The predicted depth (D) and width (W) of the lesions for each model are included in Table 3.

The extent of damage predicted by the dynamic model was ~20% larger in width and ~35% larger in depth, and almost double the area of the lesion predicted by the constant model. The largest area of damage was predicted for the dynamic properties model in which the layer of fat was incorporated, as also seen in the gross (visual) inspection of the specimens Figure 6 (a and b).

Table 3. Theoretical predictions and experimental measurements of the RF lesion size, for different models. Experimental results are given as the mean ± standard deviation of 5 experiments.

Model	Theoretical predictions		Experimental measurements (mean ± S.D.)	
	W (cm)	D (cm)	W (cm)	D (cm)
1. Static properties	2.4	1.2	N/A	N/A
2. Dynamic properties	2.9	1.8	2.7 ± 0.3	1.9 ± 0.2
3. Dynamic (with fat)	3.0	2.0	2.8 ± 0.2	2.3 ± 0.2

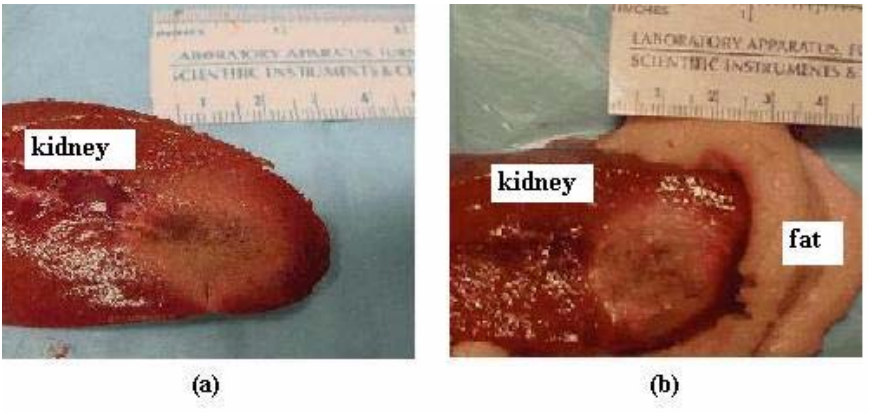

Fig. 6. Gross pathology of the RFA lesion: (a) fat not included, and (b) fat surrounding the kidney (white areas correspond to coagulation)

4 Discussion and Future Work

The deposition of RF energy is considered to be mainly resistive, i.e. the heat arises from the ionic agitation caused by the RF heating and the displacement currents are neglected [2]. The incorporation of tissue properties is known to be very important in order to accurately predict the extent of the thermal lesions [12]. As a result, the energy absorbed by tissue depends on the changes in electrical conductivity, which further affects the temperature distribution and the extent of the thermal damage, as demonstrated by comparing the results between the dynamic and static models. We calculated the thermal lesion size using Arrhenius equation instead of iso-dose temperatures, and validate it experimentally. Our results suggest that a damage model based on this formalism is more accurate for kidney tissue than a model based on temperature alone. In a study for RFA of liver [6], the authors considered a 50°C iso-contour as the margin of 'coagulated area' and an overestimation of lesion size

calculated based on the 47°C contour compared to Arrhenius model was observed. Additional evidence from theoretical and experimental results obtained in liver tissue, showed that 42-47°C isotherms give wrong estimates of the extent of the damage, and so, the iso-dose damage should be carefully considered instead of the traditional iso-dose temperature [5].

Results from our study also suggest that RF lesions produced in kidney are affected by a surrounding layer of fat acting as both an electrical and thermal insulator. Such an observation is important for clinical studies since the peri-renal fat surrounding the human kidney can have a thickness of up to 2 cm, thus the fat could protect the anatomical structures surrounding the kidney [1]. In addition, the electrode position relative to the peri-renal fat plays an important role in defining the final size and shape of the RF lesion in kidney. Preferential heating of the tumors surrounded by fat has also been demonstrated by others via simulations and experimental studies for RF ablation in breast tissue, emphasizing the importance of incorporating fat into the domain geometry for realistic simulations [12].

Our model has certain limitations. The implementation of the model was limited to a 2D case. Thus, we considered only two tines of the RF needle since it was advantageous for designing the experiment validating the temperature contours. In reality, this RF electrode has 8 tines each contributing to the lesion growth in 3D; this most likely accounts for the difference between predicted and experimentally generated thermal damage. Desiccation and contraction of the tissue may contribute to smaller dimensions obtained in the experiments versus simulations. We also limited the study to un-perfused scenarios.

In the future, we will extend the model to a 3D case and include the perfusion term in the BHT equation, as well as experimental validation in a perfused kidney model. Treatment optimization and designing new and improved heating applicators as well as their placement relative to the target (i.e., tumours), are ongoing challenges for a better thermal therapy planning [13, 14].

References

1. Stern, J.M., Svatek, R., Park, S., Hermann, M., Lotan, Y., Sagalowsky, A.I., Cadeddu, J.A.: Intermediate comparison of partial nephrectomy and RFA for clinical T1a renal tumours. British Journal of Urology 100, 287–290 (2007)
2. Thomsen, S.: Qualitative and quantitative pathology of clinically relevant thermal lesions. Critical Reviews of Optical Science and Technology CR75, 425–458 (2000)
3. Strohbehn, J.: Temperature distributions from interstitial RF electrode hyperthermia systems: theoretical prediction. Int. J. Radiation Oncology 9, 1655–1667 (1983)
4. Pop, M., Molkovski, A., Chin, L., Kolios, M., Jewett, M., Sherar, M.: Changes in dielectric properties at 460 kHz of kidney and fat: importance for radio-frequency thermal therapy. Phys. Med. Biol. 48, 2509–2525 (2003)
5. Chang, I., Nguyen, U.D.: Thermal modeling of lesion growth with radio-frequency ablation devices. Biomedical Engineering OnLine 3, 27 (2004)
6. Tungjikusolmun, S., Staelin, S.T., Haemmerich, D., et al.: 3D finite-element analyses for RF hepatic tumor ablation. IEEE Trans. Biomed. Eng. 49, 3–9 (2002)

7. Meyer, M., Velte, H., Lindenborn, H., Bangert, A., Dahlhaus, D., Albers, P.: Radiofrequency ablation in renal tumors improved by preopeartive ex-vivo computer simulation model. Journal of Endourology 21, 886–890 (2007)
8. Pennes, H.: Analysis of tissue and arterial blood temperatures in the resting forearm. Appl. Physiol. 85, 5–34 (1998)
9. Pearce, J., Thomsen, S.: Rate process analysis of thermal damage. Optical-thermal Response of Laser-Irradiated Tissue, pp. 561–605. Plenum, New York (1995)
10. Duck, F.A.: Physical Properties of Tissue, A Comprehensive Reference Book. Harcourt Brace Jovanovich, London (1990)
11. Van de Kamer, J.B., Van Wieringen, N., De Leeuw, A.C., Lagendijk, J.W.: The significance of accurate dielectric tissue data for hyperthermia treatment planning. Int. J. Hyperthermia 17, 123–142 (2001)
12. Ekstrand, V., Wiskell, H., Schultz, I., Sandtstedt, B., Rotstain, S., Eriksson, A.: Influence of electrical and thermal properties on RF ablation of breast cancer: is the tumour preferentially heated? Biomedical Engineering OnLine 4, 41 (2005)
13. Berjano, E.J.: Theoretical modelling for radio-frequency ablation state-of-the-art and challenges for the future. Biomedical Engineering OnLine 5, 24 (2006)
14. Chen, C.R., Miga, M.I., Galloway, R.L.: Optimizing Electrode Placement Using Finite-Element Models in Radiofrequency Ablation Treatment Planning. IEEE Trans. Biomed. Eng. 56, 237–245 (2009)